ELSEVIER

Physica D 133 (1999) 404–415

PHYSICA D

www.elsevier.com/locate/physd

Adaptive hierarchical modeling of heterogeneous structures

J. Tinsley Oden *, Kumar Vemaganti

Texas Institute for Computational and Applied Mathematics, The University of Texas at Austin, Austin, TX 78712, USA

Abstract

Predictability of the response of structural components to the action of external forces hinges on the selection of an appropriate mathematical and computational model of the governing physics. Invariably, this also involves decisions on what spatial and temporal scales are expected to be important in influencing the quality of the prediction. The process of model selection, particularly multiscale modeling, is not well defined and is often imprecise, heuristic, and the source of the most error in predicting physical behavior. This work presents a systematic technique for model selection and analysis of a class of multiscale problems encountered in the study of heterogeneous materials. The process, referred to as hierarchical modeling, consists of precisely characterizing a set of mathematical models of events of the smallest scale expected to influence the events of interest, and of developing rigorous *a posteriori* estimates of modeling error in the results obtained for one scale compared to models of finer scale. These estimated errors are then used in an adaptive process that automatically selects models and inherent spatial scales that produce simulations meeting preset error tolerances. The microstructures can be randomly distributed or deterministic or both, depending on the structure of models in the hierarchical set. The adaptive process can lead to models with non-uniform structure that depends upon boundary and initial data, loads and source terms, geometry, and other data. Several implementations of this process with applications to composite materials are described.

Keywords: Heterogeneous materials; Composites; Hierarchical modeling

1. Introduction

Our broad goal here is to describe computer-based procedures for automatically selecting appropriate mathematical models to study and predict certain natural phenomena, including cases in which the models themselves involve levels of uncertainty. Our approach is to develop a mathematical and ultimately a computational characterization of this broad goal and to focus on a narrow but important set of applications: the prediction of the stress, deformation and damage of highly heterogeneous materials.

Key ideas are to *adaptively* select models from a broad, often abstract class. The quality of a given model is determined by the error in the prediction it delivers compared to the most sophisticated model within its class. Thus,

* Corresponding author. Tel:. +1-512-471-3312; Fax: +1-512-471-8694

E-mail addresses: oden@ticam.utexas.edu (J. Oden), kumar@ticam.utexas.edu (K. Vemaganti)

0167-2789/99/$ – see front matter
PII: S0167-2789(99)00085-8

for example, the quality of a model exhibiting certain spatial scales will be measured by comparing the solutions it delivers to models with much finer scales —even though these fine-scale models may never be actually used. This control of quality of models, and the adaptive modeling process, is made possible through *a posteriori error estimates*, which provide computable measures of the error of coarse versus fine-scale models.

The present investigation reviews the general hierarchical modeling strategy for modeling the elastostatics of heterogeneous bodies and extends previous work [6,7,11,12] in two significant ways: firstly, we develop new procedures of a posteriori error estimation of local quantities of interest (as opposed to global energy estimates) and secondly, we briefly discuss how problems with randomly distributed constituents can be handled. Our present analysis assumes that the finest scales of interest in our hierarchical class are adequately captured by continuum theories of materials, although more general situations could conceivably be considered. We also present the results of applications to several test cases.

2. Model problem description

2.1. Elastostatics of a heterogeneous solid

We begin with a mathematical characterization of a class of models of deformation of a heterogeneous elastic body. Let $\Omega \subset \mathbb{R}^N$, $N = 1, 2, 3$, an open bounded domain with a smooth boundary, be the region in space occupied by the body. As usual, $H^1(\Omega)$ stands for the space of functions with distributional derivatives of order ≤ 1 in $L^2(\Omega)$. Let $\boldsymbol{H}^1(\Omega) \stackrel{def}{=} (H^1(\Omega))^N$ and $\boldsymbol{L}^2(\Omega) \stackrel{def}{=} (L^2(\Omega))^N$ with the usual norms.

The body is in static equilibrium under the action of body forces $\boldsymbol{f} \in \boldsymbol{L}^2(\Omega)$ and tractions $\boldsymbol{t} \in \boldsymbol{L}^2(\Gamma_t)$, where $\Gamma_t \subset \partial\Omega$. Displacements $\mathcal{U}$ are prescribed on $\Gamma_u = \partial\Omega \backslash \Gamma_t$. Let $\hat{\boldsymbol{u}} \in \boldsymbol{H}^1(\Omega)$ such that $\hat{\boldsymbol{u}}|_{\Gamma_u} = \mathcal{U}$. Next, the body is assumed to be characterized by an elasticity tensor $\boldsymbol{E} \in (L^\infty(\Omega))^{N^2 \times N^2}$ which satisfies the standard ellipticity and symmetry conditions. Let $\boldsymbol{\epsilon}$ and $\boldsymbol{\sigma}$ denote the strain and stress tensors, respectively. Then the equations governing the displacement field on Ω are

$$\begin{aligned} &-\nabla \cdot \boldsymbol{\sigma} = \boldsymbol{f} \quad \text{in } \Omega, \\ &\boldsymbol{\sigma} = \boldsymbol{E}\boldsymbol{\epsilon} \quad \text{in } \Omega, \\ &\boldsymbol{\epsilon} = \tfrac{1}{2}(\nabla \boldsymbol{u} + (\nabla \boldsymbol{u})^T) \quad \text{in } \Omega, \\ &\boldsymbol{u} = \mathcal{U} \quad \text{on } \Gamma_u, \\ &\boldsymbol{\sigma} \cdot \boldsymbol{n} = \boldsymbol{t} \quad \text{on } \Gamma_t, \end{aligned} \tag{1}$$

where $\boldsymbol{n}$ is the unit outward normal to Ω. The variational form of (1) is given by the following problem:

$$\text{Find } \boldsymbol{u} \in \{\hat{\boldsymbol{u}}\} + \boldsymbol{V}(\Omega) \text{ such that } \mathcal{B}(\boldsymbol{u}, \boldsymbol{v}) = \mathcal{F}(\boldsymbol{v}) \quad \forall \boldsymbol{v} \in \boldsymbol{V}(\Omega), \tag{2}$$

where the space of admissible functions $\boldsymbol{V}(\Omega)$ is defined as

$$\boldsymbol{V}(\Omega) \stackrel{def}{=} \{\boldsymbol{v} : \boldsymbol{v} \in \boldsymbol{H}^1(\Omega), \boldsymbol{v}|_{\Gamma_u} = \boldsymbol{0}\}. \tag{3}$$

The bilinear and linear forms are defined as

$$\mathcal{B}(\boldsymbol{u}, \boldsymbol{v}) \stackrel{def}{=} \int_\Omega \nabla \boldsymbol{v} : \boldsymbol{E} \nabla \boldsymbol{u} \, d\boldsymbol{x} = \int_\Omega \mathrm{tr}[(\nabla \boldsymbol{v})^{\mathrm{T}} \boldsymbol{E} \nabla \boldsymbol{u}] \, d\boldsymbol{x} \tag{4}$$

and

$$\mathcal{F}(\boldsymbol{v}) \stackrel{def}{=} \int_\Omega \boldsymbol{f} \cdot \boldsymbol{v} \, d\boldsymbol{x} + \int_{\Gamma_t} \boldsymbol{t} \cdot \boldsymbol{v} \, d\boldsymbol{s}. \tag{5}$$

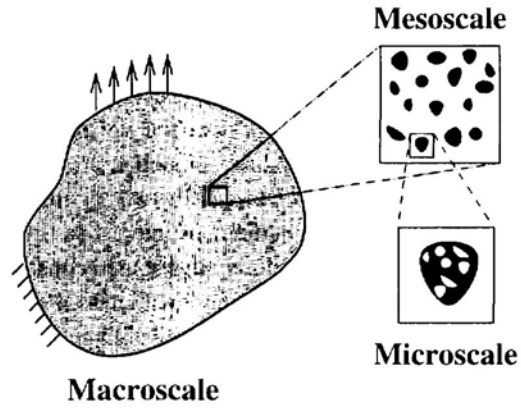

Fig. 1. The various scales seen in a composite medium.

2.2. *Homogenization and the homogenized problem*

For the type of problems considered in this paper, $\boldsymbol{E}$ is a highly oscillatory function characterizing microstructure with multiple scales, as shown in Fig. 1. Thus, the use of conventional methods, like finite elements, to solve the elasticity problem is computationally enormously expensive and in most cases, impossible. This problem can, however, be made more amenable to computation through standard homogenization processes, whereby $\boldsymbol{E}$ is replaced by a function $\boldsymbol{E}^0$, often a constant, that is designed to characterize the macroscopic behavior of the structure.

Classical homogenization techniques assume the existence of a representative volume element (RVE), the repetition of which produces the composite medium under consideration; see the works of Bensoussan et al. [2] and Sanchez-Palencia [9] for details. The overall or homogenized properties of the RVE are computed by solving a *local* periodic boundary value problem. In the recent work of Cruz and Patera [3], the RVE problem is solved by a Monte-Carlo method treating the homogenized material tensor as a continuous random variable. The result of homogenization, whether the microstructure of the composite is deterministic or otherwise, is typically an estimate of the "overall" properties of the medium. Replacing the actual microstructure $\boldsymbol{E}$ of the composite by a homogeneous material tensor $\boldsymbol{E}^0$, we arrive at the homogenized problem which reads

$$
\begin{aligned}
&-\nabla\cdot\boldsymbol{\sigma}^0 = \boldsymbol{f} \quad \text{in } \Omega,\\
&\boldsymbol{\sigma}^0 = \boldsymbol{E}^0\boldsymbol{\epsilon}^0 \quad \text{in } \Omega,\\
&\boldsymbol{\epsilon}^0 = \tfrac{1}{2}(\nabla\boldsymbol{u}^0 + (\nabla\boldsymbol{u}^0)^T) \quad \text{in } \Omega,
\end{aligned}
$$

$$
\begin{aligned}
&\boldsymbol{u}^0 = \mathcal{U} \quad \text{on } \Gamma_u,\\
&\boldsymbol{\sigma}^0\cdot\boldsymbol{n} = \boldsymbol{t} \quad \text{on } \Gamma_t
\end{aligned}
\tag{6}
$$

and the corresponding variational formulation of the homogenized problem is

$$
\text{Find } \boldsymbol{u}^0 \in \{\hat{\boldsymbol{u}}\} + \boldsymbol{V}(\Omega) \text{ such that } \mathcal{B}^0(\boldsymbol{u}^0, \boldsymbol{v}) = \mathcal{F}(\boldsymbol{v}) \quad \forall \boldsymbol{v} \in \boldsymbol{V}(\Omega) \tag{7}
$$

with

$$
\mathcal{B}^0(\boldsymbol{u}^0, \boldsymbol{v}) \overset{def}{=} \int_\Omega \nabla\boldsymbol{v} : \boldsymbol{E}^0\nabla\boldsymbol{u}^0 \,\mathrm{d}\boldsymbol{x} \tag{8}
$$

and with the right-hand side as defined in (5).

3. A posteriori error estimates and the Homogenized Dirichlet Projection Method

The homogenized solution $\boldsymbol{u}^0$ is obviously in error because material information is lost due to the process of homogenization. The homogenization or modeling error is defined as the difference between the exact solution and the homogenized solution, $\boldsymbol{e}^0 \stackrel{def}{=} \boldsymbol{u} - \boldsymbol{u}^0$.

In this section, we present a global energy measure of the modeling error and describe the Homogenized Dirichlet Projection Method (HDPM). We discuss how the HDPM can be extended to include the effects of uncertainty and randomness of microstructure. Also, we present a new technique for estimating the modeling error in quantities of interest that can be represented as continuous linear functionals on the space of admissible functions $\boldsymbol{V}$.

3.1. An energy estimate of the homogenization error

The following theorem is proved in [12].

Theorem 1. *Let $\boldsymbol{u}$ and $\boldsymbol{u}^0$ be the solutions to problems (2) and (7), respectively. Then the following holds:*

$$||\boldsymbol{e}^0||^2_{E(\Omega)} = ||\boldsymbol{u} - \boldsymbol{u}^0||^2_{E(\Omega)} \leq \zeta^2 \stackrel{def}{=} \int_{\Omega} \mathcal{I}_0 \nabla \boldsymbol{u}^0 : \boldsymbol{E} \mathcal{I}_0 \nabla \boldsymbol{u}^0 \, \mathrm{d}\boldsymbol{x}, \tag{9}$$

where

$$\mathcal{I}_0 \stackrel{def}{=} (\mathbf{I} - \boldsymbol{E}^{-1} \boldsymbol{E}^0). \tag{10}$$

Thus, the homogenization error can be predicted knowing only the homogenized solution $\boldsymbol{u}^0$, the actual microstructure $\boldsymbol{E}$ and the homogenized material tensor $\boldsymbol{E}^0$.

3.2. The Homogenized Dirichlet Projection Method

We begin by noting that the homogenized solution $\boldsymbol{u}^0$ can in general be a poor approximation to $\boldsymbol{u}$. In order to develop a systematic and rigorous way of improving the homogenized solution, we consider a non-overlapping partition $\mathcal{P}$ of the domain Ω into subdomains Θ_k, $k = 1, \ldots, N(\mathcal{P})$. The boundary $\partial\Theta_k$ of each subdomain Θ_k consists of a portion Γ_{k_t} on which tractions are prescribed and a portion Γ_{k_u} on which displacements are prescribed

$$\Gamma_{k_t} = \Gamma_t \cap \partial\Theta_k, \qquad \Gamma_{k_u} = \partial\Theta_k \backslash \Gamma_u. \tag{11}$$

Local function spaces are defined as

$$\boldsymbol{V}(\Theta_k) \stackrel{def}{=} \{\boldsymbol{v} : \boldsymbol{v} \in \boldsymbol{V}(\Omega), \boldsymbol{v}|_{\Omega \backslash \bar{\Theta}_k} = \mathbf{0}, \boldsymbol{v}|_{\Gamma_{k_u}} = \mathbf{0}\}. \tag{12}$$

For each subdomain, we define an operator $\mathcal{E}_k$ that extends functions from the local space $\boldsymbol{V}(\Theta_k)$ to $\boldsymbol{V}(\Omega)$ as follows:

$$\mathcal{E}_k : \boldsymbol{V}(\Theta_k) \ni \boldsymbol{v}_k \to \boldsymbol{v} \in \boldsymbol{V}(\Omega), \quad \boldsymbol{v}|_{\Theta_k} \stackrel{def}{=} \boldsymbol{v}_k, \quad \boldsymbol{v}|_{\Omega \backslash \Theta_k} = \mathbf{0}. \tag{13}$$

The restriction of the homogenized solution to each subdomain is defined as $\boldsymbol{u}_k^0 \stackrel{def}{=} \boldsymbol{u}^0|_{\Theta_k}$. We denote by $\tilde{\boldsymbol{u}}_k$ the solution to the following boundary value problem:

$$\text{Find } \tilde{\boldsymbol{u}}_k \in \{\boldsymbol{u}_k^0\} + \boldsymbol{V}(\Theta_k) \text{ such that } \mathcal{B}_k(\tilde{\boldsymbol{u}}_k, \boldsymbol{v}_k) = \mathcal{F}_k(\boldsymbol{v}_k) \quad \forall \boldsymbol{v}_k \in \boldsymbol{V}(\Theta_k), \tag{14}$$

for $1 \leq k \leq N(\mathcal{P})$ with

$$\mathcal{B}_k(\tilde{\boldsymbol{u}}_k, \boldsymbol{v}_k) \stackrel{def}{=} \int_{\Theta_k} \nabla \boldsymbol{v}_k : \boldsymbol{E} \nabla \tilde{\boldsymbol{u}}_k \, \mathrm{d}\boldsymbol{x} \tag{15}$$

and

$$\mathcal{F}_k \stackrel{def}{=} \int_{\Theta_k} \boldsymbol{f} \cdot \boldsymbol{v}_k \, \mathrm{d}\boldsymbol{x} + \int_{\Gamma_{k_t}} \boldsymbol{t} \cdot \boldsymbol{v}_k \, \mathrm{d}\boldsymbol{s}. \tag{16}$$

The displacements on Γ_{k_u} are prescribed as $\tilde{\boldsymbol{u}}_k|_{\Gamma_{k_u}} = \boldsymbol{u}_k^0|_{\Gamma_{k_u}}$, i.e., the homogenized solution is used as Dirichlet data on the Γ_{k_u} portion of each subdomain's boundary. In particular, this data is used on the interior part of each subdomain's boundary given by $\partial\Theta \backslash \partial\Omega$. As a result, the local problems are uncoupled. Finally, a global solution is constructed from the local solutions in the following manner:

$$\tilde{\boldsymbol{u}} \stackrel{def}{=} \boldsymbol{u}^0 + \sum_{k=1}^{N(\mathcal{P})} \mathcal{E}_k(\tilde{\boldsymbol{u}}_k - \boldsymbol{u}_k^0), \quad \tilde{\boldsymbol{u}} \in \{\hat{\boldsymbol{u}}\} + \boldsymbol{V}(\Omega). \tag{17}$$

which will be referred to as the HDPM solution. Clearly, this new solution is continuous across subdomains. The following result from [7] guarantees that the HDPM solution is indeed an improved solution.

Theorem 2. *With the previous definitions in force,*

$$\mathcal{J}(\tilde{\boldsymbol{u}}) \leq \mathcal{J}(\boldsymbol{u}^0), \tag{18}$$

and hence

$$||\boldsymbol{u} - \tilde{\boldsymbol{u}}||_{E(\Omega)} \leq ||\boldsymbol{u} - \boldsymbol{u}^0||_{E(\Omega)}, \tag{19}$$

where $\mathcal{J}(\boldsymbol{v}) \stackrel{def}{=} \frac{1}{2}\mathcal{B}(\boldsymbol{v}, \boldsymbol{v}) - \mathcal{F}(\boldsymbol{v})$ *is the potential energy of* $\boldsymbol{v}$.

Proof of two corollaries that follow immediately from this theorem are also in [7].

Corollary 3. *Let* $\boldsymbol{u}$ *be the exact solution to (2). Additionally, assume that* $\nabla \cdot (\boldsymbol{E}\nabla\tilde{\boldsymbol{u}}_k)$, $\boldsymbol{f} \in \boldsymbol{H}^{-1}(\Theta_k)$ *and* $(\boldsymbol{E}\nabla\tilde{\boldsymbol{u}}_k) \cdot \boldsymbol{n} \in \boldsymbol{H}^{-1/2}(\Gamma_{k_u})$. *Then,*

$$||\boldsymbol{u} - \tilde{\boldsymbol{u}}||^2_{E(\Omega)} \leq \psi^2 \stackrel{def}{=} 2(\mathcal{J}(\tilde{\boldsymbol{u}}) - \mathcal{J}(\boldsymbol{u}^0)) + \zeta^2. \tag{20}$$

This result provides an *a posteriori* estimate of the error in the improved solution $\tilde{\boldsymbol{u}}$ compared to the fine-scale solution $\boldsymbol{u}$. It can be seen that the term $(\mathcal{J}(\tilde{\boldsymbol{u}}) - \mathcal{J}(\boldsymbol{u}^0))$ is negative so that $\psi \leq \zeta$ always. The next result is a very useful sensitivity property.

Corollary 4. *Define* ζ_k *by*

$$\zeta_k^2 \stackrel{def}{=} \int_{\Theta_k} \mathcal{I}_0 \nabla \boldsymbol{u}^0 : \boldsymbol{E}\mathcal{I}_0 \nabla \boldsymbol{u}^0 \, \mathrm{d}\boldsymbol{x} \tag{21}$$

and $\tilde{\boldsymbol{e}}_k^0$ *by* $\tilde{\boldsymbol{e}}_k^0 \stackrel{def}{=} \tilde{\boldsymbol{u}}_k - \boldsymbol{u}_k^0$. *Then, for* $1 \leq k \leq N(\mathcal{P})$,

$$\|\tilde{\boldsymbol{e}}_k^0\|_{E(\Theta_k)} = \|\tilde{\boldsymbol{u}}_k - \boldsymbol{u}_k^0\|_{E(\Theta_k)} \leq \zeta_k. \tag{22}$$

The above corollary allows us to predict the improvement that can be obtained by solving the local problem(s) (14) for the fine-scale corrections $\tilde{\boldsymbol{u}}_k$ over each subdomain Θ_k. If ζ_k is small in a subdomain, then there is little

gained by solving a local problem. On the other hand, if the above estimate is sharp, and ζ_k is high in a subdomain, the homogenized solution can be significantly improved by solving the local problem (14). Finally, we present the overall computational algorithm of the HDPM.

Step 1. Given the initial data Ω, Γ_u, Γ_t, $\boldsymbol{E}$, $\boldsymbol{f}$, $\hat{\boldsymbol{u}}$ and t, construct a partition of the domain $\mathcal{P} = \{\Theta_k\}_{k=1}^{N}$. Choose a homogenized material tensor $\boldsymbol{E}^0$. Specify sensitivity and error tolerances α_1 and α_2 so that

$$(\zeta_k)_{\text{tol}} \overset{def}{=} \alpha_1 \|\boldsymbol{u}^0\|_{E(\Omega)} \times \frac{|\Theta_k|}{|\Omega|}, \qquad \psi_{\text{tol}} \overset{def}{=} \alpha_2 \|\boldsymbol{u}^0\|_{E(\Omega)}. \tag{23}$$

Step 2. Solve the homogenized problem (7) to obtain $\boldsymbol{u}^0$.

Step 3. Compute the local sensitivities ζ_k using (21) for $k = 1, \ldots, N(\mathcal{P})$ and form a set $\mathcal{K}$ of subdomains which are above the prescribed sensitivity tolerance

$$\mathcal{K} = \{k : \zeta_k \geq (\zeta_k)_{\text{tol}}\}. \tag{24}$$

Step 4. For the subdomains that fail to satisfy the sensitivity tolerance, $k \in \mathcal{K}$, solve the local problems (14) to obtain $\tilde{\boldsymbol{u}}_k$.

Step 5. Construct the HDPM solution

$$\tilde{\boldsymbol{u}} = \boldsymbol{u}^0 + \sum_{k \in \mathcal{K}} \mathcal{E}_k (\tilde{\boldsymbol{u}}_k - \boldsymbol{u}_k^0). \tag{25}$$

Step 6. Compute the estimated error in the HDPM solution

$$\psi \overset{def}{=} [2(\mathcal{J}(\tilde{\boldsymbol{u}}) - \mathcal{J}(\boldsymbol{u}^0)) + \zeta^2]^{1/2}. \tag{26}$$

Step 7. If $\psi \leq \psi_{\text{tol}}$, STOP. Else, repeat Steps 2–7 with improved material properties. A general algorithm for choosing improved properties can be found in [7]. If the error tolerance is not satisfied with improved material properties, go to Step 8.

Step 8. Coarsen the partition and repeat Steps 2–7.

Step 9. Relaxation (this step is optional). At the conclusion of the adaptive process when all global and subdomain errors meet the assigned tolerances, tractions are discontinuous across subdomain boundaries. A number of Schwartz-type iterations relaxing the boundary constraints on displacements can be performed to reduce the stress discontinuity, remove spurious singularities in the displacement derivatives, and further improve the accuracy of local features of the solution.

3.3. Hierarchical treatment of uncertainty and randomness in composites

The analysis in this section has thus far assumed that the microstructure of the composite $\boldsymbol{E}$ is known. This assumption is reasonable when this data can be obtained, for instance, by imaging techniques such as Computer Tomography. Details of such techniques are described in [4,10]. When this data is not available or when it is known that such data displays large statistical dispersion, one needs to include the effects of uncertainty in the analysis. This can be easily achieved in the framework of hierarchical modeling by using, say, a Monte-Carlo scheme. A model that is governed by (1), but with material coefficients that are random variables, is treated as the finest scale model in the hierarchy of models. Each Monte-Carlo realization of the random microstructure is treated as the next model in the hierarchy. Finally, the homogenized treatment of each realization constitutes the coarsest model of the hierarchy.

This hierarchy of models corresponds to the use of the HDPM, as described earlier, to solve each realization of the Monte-Carlo scheme. Moreover, the inherent parallelism present in Monte-Carlo schemes makes such a hierarchy

computationally desirable. By using an ample number of realizations, requisite statistical moments of various physical quantities, such as maximum stress, maximum deformation, damage variables, etc., can be computed.

3.4. Estimation of homogenization error in quantities of interest

Recent work in error estimation in the context of finite element analysis has focused on obtaining bounds on the numerical error in quantities of interest other than the energy norm [1,8]. In this section, we use an approach suggested by the techniques for approximation error estimation of Prudhomme and Oden [8] to obtain an estimate of the homogenization error in other quantities. We assume that we are interested in estimating $L(\boldsymbol{e}^0) = L(\boldsymbol{u}) - L(\boldsymbol{u}^0)$, where L is a continuous linear functional on $\boldsymbol{V}(\Omega)$, $L \in \boldsymbol{V}'$. Some examples of such a functional are

$$L(\boldsymbol{u}) = \int_{\Gamma} \boldsymbol{u} \cdot \boldsymbol{n} \, \mathrm{d}\boldsymbol{x}, \quad \Gamma \subset \partial\Omega, \qquad L(\boldsymbol{u}) = \int_{B(\boldsymbol{x}_0,\epsilon)} k_\epsilon(\boldsymbol{x}; \boldsymbol{x}_0)\sigma_{ij}(\boldsymbol{u}) \, \mathrm{d}\boldsymbol{x}, \quad \boldsymbol{x}_0 \in \Omega, \quad 1 \le i, j \le N, \tag{27}$$

where $B(\boldsymbol{x}_0, \epsilon)$ is an open ball of radius ϵ centered at $\boldsymbol{x}_0$, and $k_\epsilon(\boldsymbol{x}; \boldsymbol{x}_0)$ is an infinitely smooth mollifier (see Example 3 and [5]).

We note that the homogenization error is governed by the following equation:

$$\text{Find } \boldsymbol{e}^0 \in \boldsymbol{V}(\Omega) \text{ such that } \mathcal{B}(\boldsymbol{e}^0, \boldsymbol{v}) = \mathcal{R}^0(\boldsymbol{v}) \stackrel{def}{=} -\int_{\Omega} \nabla \boldsymbol{v} : \boldsymbol{E}\mathcal{I}_0 \nabla \boldsymbol{u}^0 \quad \forall \boldsymbol{v} \in \boldsymbol{v}(\Omega). \tag{28}$$

The main objective here is to relate $L(\boldsymbol{e}^0)$ to the "source" of the homogenization error, $\mathcal{R}^0$. So, we would like to find a linear functional $\mathcal{W} \in \boldsymbol{V}''$, if it exists, such that

$$L(\boldsymbol{e}^0) = \mathcal{W}(\mathcal{R}^0) = \langle \mathcal{W}, \mathcal{R} \rangle_{\boldsymbol{V}'' \times \boldsymbol{V}'}. \tag{29}$$

The functional $\mathcal{W}$ is known as the influence function(al) since it indicates the influence of the residual on the quantity of interest. Since, $\boldsymbol{V}$ is reflexive (every Hilbert space is reflexive), we have that $\exists\, !\boldsymbol{w} \in \boldsymbol{V}$ such that

$$\langle \mathcal{R}, \boldsymbol{w} \rangle_{\boldsymbol{V}' \times \boldsymbol{V}} = \langle \mathcal{W}, \mathcal{R} \rangle_{\boldsymbol{V}'' \times \boldsymbol{V}'} \tag{30}$$

and hence (29) becomes

$$L(\boldsymbol{e}^0) = \mathcal{R}^0(\boldsymbol{w}). \tag{31}$$

Using (28), we obtain

$$L(\boldsymbol{e}^0) = \mathcal{B}(\boldsymbol{e}^0, \boldsymbol{w}). \tag{32}$$

The influence function $\boldsymbol{w}$ can thus be obtained as a solution to the global dual problem

$$\text{Find } \boldsymbol{w} \in \boldsymbol{V}(\Omega) \text{ such that } \mathcal{B}(\boldsymbol{v}, \boldsymbol{w}) = L(\boldsymbol{v}) \quad \forall \boldsymbol{v} \in \boldsymbol{V}(\Omega). \tag{33}$$

It then follows that $\boldsymbol{w}$ exists and is unique. The dual problem (33), however, is as difficult to solve as the original problem (2). A natural way to simplify this problem is to solve the homogenized dual problem

$$\text{Find } \boldsymbol{w}^0 \in \boldsymbol{V}(\Omega) \text{ such that } \mathcal{B}^0(\boldsymbol{v}, \boldsymbol{w}^0) = L(\boldsymbol{v}) \quad \forall \boldsymbol{v} \in \boldsymbol{V}(\Omega). \tag{34}$$

It immediately follows that the modeling error in the influence function $\bar{\boldsymbol{e}}^0 \stackrel{def}{=} \boldsymbol{w} - \boldsymbol{w}^0$ satisfies

$$\mathcal{B}(\boldsymbol{v}, \bar{\boldsymbol{e}}^0) = \bar{\mathcal{R}}^0(\boldsymbol{v}) \quad \forall \boldsymbol{v} \in \boldsymbol{V}(\Omega), \tag{35}$$

with

$$\bar{\mathcal{R}}^0(v) = -\int_\Omega \nabla w^0 : \boldsymbol{E}\mathcal{I}_0\nabla v \, \mathrm{d}x. \tag{36}$$

We also note that $\bar{e}^0$ satisfies the following bound (analogous to (9)):

$$||\bar{e}^0||^2_{E(\Omega)} = ||w - w^0||^2_{E(\Omega)} \leq \bar{\zeta}^2 \stackrel{def}{=} \int_\Omega \mathcal{I}_0\nabla w^0 : \boldsymbol{E}\mathcal{I}_0\nabla w^0 \, \mathrm{d}x. \tag{37}$$

Returning to (32), we see that the functions e^0 and w are not known. Hence, we use the HDPM approximations of these functions to obtain the expression

$$L(e^0) \approx \beta \stackrel{def}{=} \mathcal{B}(\bar{e}^0, \bar{w}^0). \tag{38}$$

In our analysis above, we assume that the homogenization parameters chosen for the dual problem are the same as the ones chosen for the primal (original) problem. As a result, the two problems have the same left-hand side which is computationally convenient. This assumption, however, can be relaxed without major changes to our analysis. Indeed, this may not be an unattractive choice considering the fact that the homogenized problem typically requires far fewer degrees of freedom than the fine-scale problem.

4. Numerical examples

4.1. Example 1

We study on the performance of the estimate (38) for the following 1D problem. Consider an elastic bar of unit length fixed at both ends and subjected to a constant body force. The primal fine-scale and homogenized problems are $-(E(x)u'(x))' = -1, u(0) = u(1) = 0$ and $-(E^0_{\mathrm{p}}(x)u^{0'}(x))' = -1, u^0(0) = u^0(1) = 0$, E^0_{p} being the homogenized coefficient for the primal problem. The linear functional we consider is

$$L(v) = \int_a^b \sigma(v) \, \mathrm{d}x, \quad (a, b) = (0.75, 0.76), \tag{39}$$

meaning that we are interested in the local (scaled) average value of the homogenization error in the stress in the given interval. The dual fine-scale problem is then

$$-\frac{\mathrm{d}}{\mathrm{d}x}\left(E(x)\frac{\mathrm{d}w}{\mathrm{d}x}\right) = \frac{\mathrm{d}}{\mathrm{d}x}(E(x)(H(x-a) - H(x-b))), \quad w(0) = 0, \quad w(1) = 0, \tag{40}$$

and the homogenized problem is obtained by replacing $E(x)$ by $E^0_{\mathrm{d}}(x)$ (d for "dual") and w by w^0 in (40).

The unit interval is divided into 10 000 equal intervals, and for each interval the material property is chosen at random to be either $E = 1$ or $E = \tau$, where τ is the mismatch ratio. Equal amounts of hard and soft material are used. All of the following calculations are performed analytically. Also, E^0_{p} and E^0_{d} are independently chosen to be the arithmetic average $\langle E \rangle$ or the harmonic average $\langle E^{-1} \rangle^{-1}$. Finally, we define the effectivity index by $\eta \stackrel{def}{=} L(e^0)/\beta$.

Table 1 shows the effectivity indices obtained using expression (38) when the domain is divided into 10 subdomains. Of the two sets of effectivity indices shown, the first column corresponds to the case when a single local solve is performed on the subdomain containing the region of interest. To obtain the second column of effectivity indices,

Table 1
Effectivity indices for $L(v) = \int_a^b \sigma(v)\,dx$, $(a, b) = (0.75, 0.76)$, with 10 subdomains

τ	E_p^0	E_d^0	$L(e^0)$	η	η (relaxation)
10	$\langle E^{-1}\rangle^{-1}$	$\langle E^{-1}\rangle^{-1}$	−0.011869	1.07	1.03
10	$\langle E^{-1}\rangle^{-1}$	$\langle E\rangle$	−0.011869	1.07	1.04
10	$\langle E\rangle$	$\langle E^{-1}\rangle^{-1}$	−0.001694	2.31	1.35
10	$\langle E\rangle$	$\langle E\rangle$	−0.001694	2.31	1.53
100	$\langle E^{-1}\rangle^{-1}$	$\langle E^{-1}\rangle^{-1}$	−0.1257	1.01	1.00
100	$\langle E^{-1}\rangle^{-1}$	$\langle E\rangle$	−0.1257	1.01	1.00
100	$\langle E\rangle$	$\langle E^{-1}\rangle^{-1}$	−0.002029	2.45	1.36
100	$\langle E\rangle$	$\langle E\rangle$	−0.002029	2.45	2.17

Table 2
Effectivity indices for $L(v) = \int_a^b \sigma(v)\,dx$, $(a, b) = (0.75, 0.76)$, with five subdomains

τ	E_p^0	E_d^0	$L(e^0)$	η	η (relaxation)
10	$\langle E^{-1}\rangle^{-1}$	$\langle E^{-1}\rangle^{-1}$	−0.011869	1.04	1.03
10	$\langle E^{-1}\rangle^{-1}$	$\langle E\rangle$	−0.011869	1.04	1.04
10	$\langle E\rangle$	$\langle E^{-1}\rangle^{-1}$	−0.001694	2.09	1.40
10	$\langle E\rangle$	$\langle E\rangle$	−0.001694	2.09	1.60
100	$\langle E^{-1}\rangle^{-1}$	$\langle E^{-1}\rangle^{-1}$	−0.1257	1.00	1.00
100	$\langle E^{-1}\rangle^{-1}$	$\langle E\rangle$	−0.1257	1.00	1.00
100	$\langle E\rangle$	$\langle E^{-1}\rangle^{-1}$	−0.002029	2.24	1.43
100	$\langle E\rangle$	$\langle E\rangle$	−0.002029	2.24	2.11

we perform flux equilibration or relaxation (see Step 9 of the HDPM algorithm). Table 2 shows the effectivity indices obtained when the partition of the domain is coarsened to five subdomains.

From these tables, it is seen that by solving a single local problem, we obtain effectivity indices that are O(1) and in most cases close to unity. Relaxation of fluxes at subdomain boundaries improves the accuracy of the estimate, as does a coarsening of the partition.

4.2. Example 2

In this 2D example, we study the deformation of a unit square composite body assuming plane stress conditions. A schematic of the problem is shown in Fig. 2(a) with a partition consisting of four subdomains. The body is fixed on one edge and non-zero tractions are prescribed on a portion of $\partial\Omega$ we will refer to as Γ_t^*. The inclusions are assumed to be five times stiffer than the matrix material. We are interested in estimating the modeling error in the quantity

$$L(\boldsymbol{u}) = \int_{\Gamma_t^*} \boldsymbol{u}\cdot\boldsymbol{n}\,d\boldsymbol{s}. \tag{41}$$

To obtain a reference solution, we employ an overkill *hp*-adapted finite element mesh shown in Fig. 2(b) with about 60 000 degrees of freedom. We shall refer to this solution as the "exact" solution and use it compute the effectivity indices of the error estimates (9), (20) and (22).

To homogenize the problem, we use the Hashin–Shtrikman bounds and an adapted *hp* mesh used to solve (7) so as to produce an approximate solution with an estimated error of 1% in the $\boldsymbol{E}^0$-energy norm. This required only about 4600 degrees of freedom.

The sensitivity parameters ζ_k and $\bar{\zeta}_k$, $k = 1, \ldots, 4$, are computed and the effectivity indices range between 0.9 and 1.2. Using the HDPM algorithm, it is found that the subdomains that require local solves are $\mathcal{K} = \{1, 3\}$. The global energy error indicators ζ and $\bar{\zeta}$ both have an effectivity index of 1.15, and the global indicator ψ has an

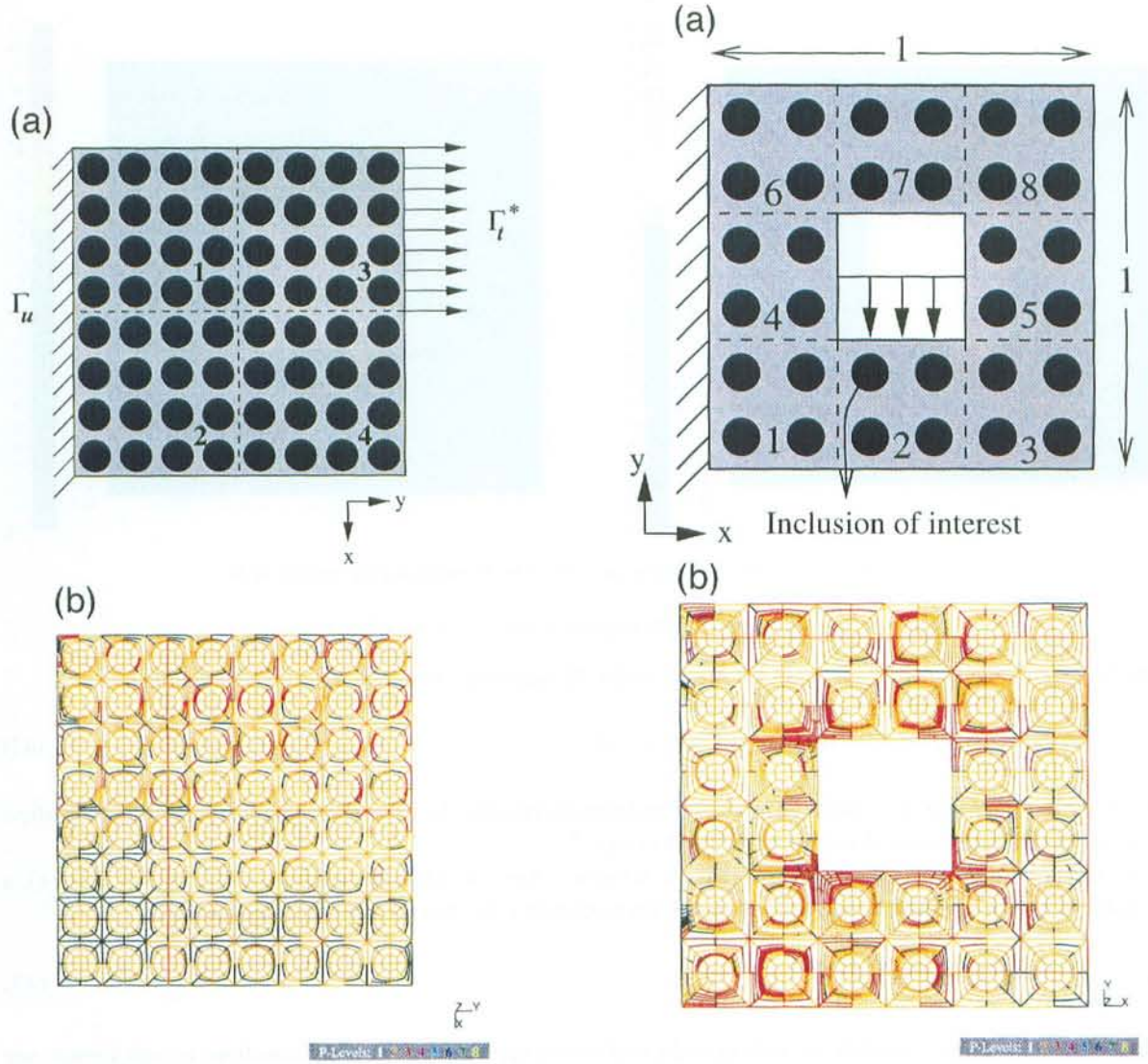

Fig. 2. (a) A test problem in two dimensions and (b) overkill mesh employed to generate the reference solution for the test problem.

Fig. 3. (a) Schematic of the test problem for stress mollification and (b) overkill *hp* mesh employed to obtain the reference solution to this problem.

effectivity index of 1.2. Finally, the effectivity index for the quantity of interest defined as $L(\tilde{\boldsymbol{u}})/L(\boldsymbol{u})$ is found to be 0.92, whereas the effectivity index for the modeling error in the quantity of interest defined as $L(\tilde{\boldsymbol{e}})/L(\boldsymbol{e}^0)$ is found to be 0.5.

4.3. Example 3

This example focuses on the estimation of modeling error in quantities of interest that represent components of the stress tensor. Mathematically, we cannot refer to pointwise values of the stress tensor as they often do not exist

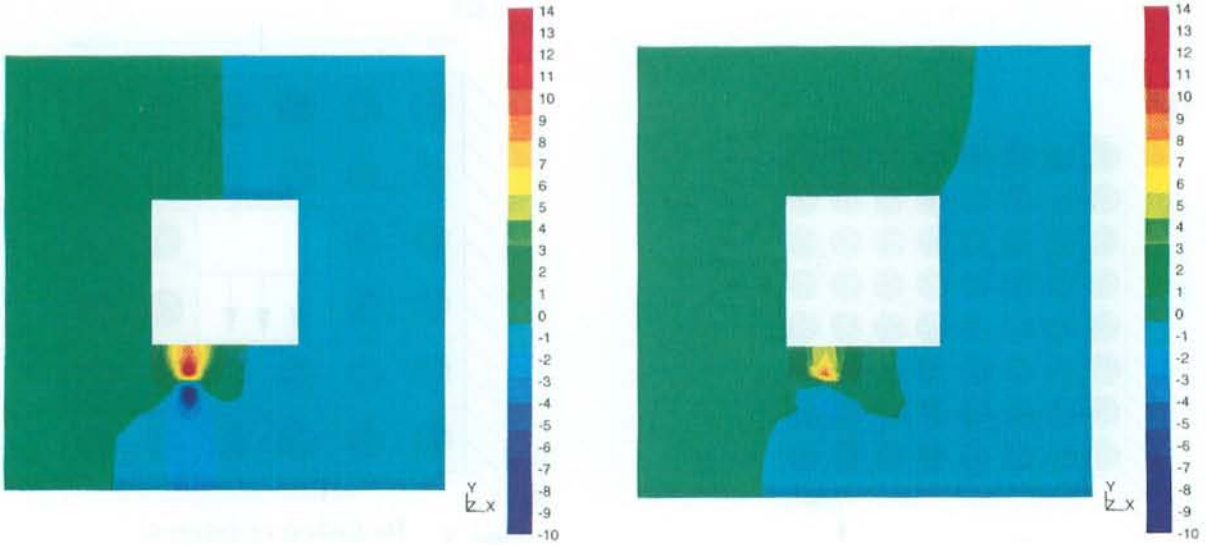

Fig. 4. The y component of the influence function $\boldsymbol{w}$ obtained using the overkill mesh.

Fig. 5. The y component of the homogenized influence function $\boldsymbol{w}^0$ for Example 3.

and because $\boldsymbol{\sigma}_{ij}(\boldsymbol{u})(\boldsymbol{x}_0) \notin \boldsymbol{V}'$, $\boldsymbol{x}_0 \in \Omega$. Hence we define the quantity of interest in terms of a *mollifier*

$$L(\boldsymbol{u}) = \int_{\operatorname{supp} k_\epsilon} k_\epsilon(\boldsymbol{x}; \boldsymbol{x}_0)\sigma_{ij}(\boldsymbol{u})\,\mathrm{d}\boldsymbol{x}, \quad 1 \le i, j \le N, \tag{42}$$

where the mollifier $k_\epsilon(\boldsymbol{x}; \boldsymbol{x}_0)$, centered at $\boldsymbol{x}_0 \in \Omega$ and characterized by the parameter ϵ, has the following properties:

- $k_\epsilon(\boldsymbol{x}; \boldsymbol{x}_0)$ has continuous derivatives of all orders on $\mathbb{R}^N$.
- $k_\epsilon(\boldsymbol{x}; \boldsymbol{x}_0) = 0$ for $|\boldsymbol{x} - \boldsymbol{x}_0| \ge \epsilon$ and $k_\epsilon(\boldsymbol{x}; \boldsymbol{x}_0) > 0$ for $|\boldsymbol{x} - \boldsymbol{x}_0| < \epsilon$. Thus, the support of $k_\epsilon(\boldsymbol{x}; \boldsymbol{x}_0)$ is $B(\boldsymbol{x}_0, \epsilon)$, a ball of radius ϵ centered at $\boldsymbol{x}_0$. Also, all partial derivatives of $k_\epsilon(\boldsymbol{x}; \boldsymbol{x}_0)$ are zero outside $B(\boldsymbol{x}_0, \epsilon)$.
- $$\int_{B(\boldsymbol{x}_0,\epsilon)} k_\epsilon(\boldsymbol{x}, \boldsymbol{x}_0) = 1. \tag{43}$$

The use of mollifiers to generate smooth and arbitrarily close approximations of $\boldsymbol{L}^p$ functions is well known; see [5]. Mollification can be viewed as an averaging process over the support of the mollifier. A standard example of a mollifier is

$$k_\epsilon(\boldsymbol{x}; \boldsymbol{x}_0) = \begin{cases} c_0\ \mathrm{e}^{\epsilon^2/(|\boldsymbol{x}-\boldsymbol{x}_0|^2-\epsilon^2)}, & |\boldsymbol{x} - \boldsymbol{x}_0| < \epsilon, \\ 0, & |\boldsymbol{x} - \boldsymbol{x}_0| \ge \epsilon, \end{cases} \tag{44}$$

where the constant c_0 is chosen such that the condition (43) is satisfied.

We consider a test problem depicted by the schematic in Fig. 3(a). The structure is loaded as shown and the inclusions are five times as stiff as the matrix material. Additionally, we assume that plane stress conditions exist. We are interested in estimating the modeling error in the σ_{yy} component of the stress tensor in the inclusion indicated in Fig. 3(a). Hence, the quantity of interest is defined as

$$L(\boldsymbol{u}) = \int_{B(\boldsymbol{x}_0,\epsilon)} k_\epsilon(\boldsymbol{x}; \boldsymbol{x}) \left(D_1(\boldsymbol{x})\frac{\partial u_1}{\partial x_1} + D_2(\boldsymbol{x})\frac{\partial u_2}{\partial x_2} \right) \mathrm{d}\boldsymbol{x} \tag{45}$$

with $\boldsymbol{x} = (0.41\bar{6}, 0.25)$ and $\epsilon = 0.028$ so that the support of the mollifier lies inside the inclusion of interest. Here D_1 and D_2 represent appropriate material constants.

Fig. 3(b) shows the overkill mesh with about 70 000 degrees of freedom used to obtain a reference solution. The y component of the influence function $\boldsymbol{w}$ resulting from the overkill mesh is shown in Fig. 4. Clearly, the quantity of interest (expressed as a linear functional) acts as a local source term, and its effect is rather localized.

Accurate approximations of the homogenized solutions $\boldsymbol{u}^0$, $\boldsymbol{w}^0$ are then produced and the local sensitivity indicators ζ_k, $\bar{\zeta}_k$ are computed for $1 \leq k \leq 8$. The y component of the homogenized influence function $\boldsymbol{w}^0$ is shown in Fig. 5. The homogenized influence function, obviously, does not display all the features exhibited by the reference solution, but the effect of the mollification is clearly seen. Based on the HDPM algorithm, we find that subdomain 2 alone needs a local solve. The local problem (14) is solved on subdomain 2 and using (38), we find that modeling error in the quantity of interest is predicted with an effectivity index of 0.89, while the quantity of interest itself is predicted with an effectivity index of 0.92.

5. Final comments

We have demonstrated that the notion of adaptive hierarchical modeling can be applied successfully to highly heterogeneous media. The modeling error in modeling specific quantities of interest, such as local stresses, can be adaptively controlled to yield results very close to the exact fine-scale values, with effectivity indices η near unity in most cases. Preliminary two-dimensional calculations have been done and extensions to significant three-dimensional, nonlinear dynamic cases are thought to be feasible.

Acknowledgements

We gratefully acknowledge the support of this work by the Office of Naval Research under grant N00014-95-1-0401. Our computations were supported by NPACI, the National Partnership for Advanced Computational Infrastructure, under NSF Grant 10152711.

References

[1] I. Babuška, T. Strouboulis, C.S. Upadhyay, S.K. Gangaraj, Int. J. Numer. Meth. Engrg. 38 (1995) 4207.
[2] A. Bensoussan, J.L. Lions, G. Papanicolaou, Asymptotic Analysis for Periodic Structures, Studies in Mathematics and its Applications, vol. 5, North-Holland, Amsterdam, 1978.
[3] M.E. Cruz, A.T. Patera, Int. J. Numer. Meth. Engrg. 38 (1995) 1087.
[4] B. London, R.N. Yancey, J.A. Smith, Mater. Evaluation 48 (1990) 604.
[5] J.T. Oden, J.N. Reddy, An Introduction to the Mathematical Theory of Finite Elements, Wiley, New York, 1976.
[6] J.T. Oden, K. Vemaganti, N. Moës, Comput. Meth. Appl. Mech. Engrg 172 (1999) 3–25.
[7] J.T. Oden, T.I. Zohdi, Comput. Meth. Applied Mech. Engng. 148 (1997) 367.
[8] S. Prudhomme, J.T. Oden, Comput. Meth. Appl. Mech. Engrg., to appear.
[9] E. Sanchez-Palencia, Non-homogeneous Media and Vibration Theory, Lecture Notes in Physics, vol. 27, Springer, Berlin, 1980.
[10] K. Terada, T. Miura, N. Kikuchi, Comput. Mech. 20 (1997) 331.
[11] T.I. Zohdi, Analysis and Adaptive Modeling of Highly Heterogeneous Elastic Structures, Ph.D. Dissertation, The University of Texas at Austin, 1997.
[12] T.I. Zohdi, J.T. Oden, G.J. Rodin, Comput. Meth. Appl. Mech. Engrg. 138 (1996) 273.